ELSEVIER

Earth and Planetary Science Letters 186 (2001) 437–450

EPSL

www.elsevier.com/locate/epsl

Archeomagnetism of potsherds from Grand Banks, Ontario: a test of low paleointensities in Ontario around A.D. 1000

Claire Carvallo *, David J. Dunlop

Geophysics, Physics Department, University of Toronto at Mississauga, Mississauga, Ont., Canada L5L 1C6

Received 30 October 2000; received in revised form 25 January 2001; accepted 25 January 2001

Abstract

An archeomagnetic study was carried out on 24 pottery fragments from Grand Banks, southern Ontario. ^{14}C dating on maize found in the same pit as the potsherds gives an age in the range A.D. 990–1160 (modal age A.D. 1030). Hysteresis measurements indicate that the natural remanent magnetization is carried by pseudosingle-domain magnetite grains. Paleointensity experiments were done on 63 samples using a Thellier-type double-heating method. Half of the samples were heated in helium and the other half in air. Hysteresis measurements on samples after heating to various temperatures reveal only slight mineralogical changes during heating steps. Thirty reliable results give a paleofield intensity of 42.0 ± 7.4 μT, and a virtual axial dipole moment of $7.0 \pm 1.3 \times 10^{22}$ Am^2. This result is in agreement with the low virtual axial dipole moment values given by studies on material from Ontario compared to the values from the southwestern USA in the interval A.D. 900–1400.

Keywords: paleomagnetism; paleointensity; dipole moment; anisotropy; magnetic hysteresis

1. Introduction

Paleomagnetic records from archeological materials complement the secular variation records of absolute paleointensity and geomagnetic field direction for historical times. Most archeomagnetic studies have concentrated on sites in Europe; only four studies have been published for northeastern North America [1–4]. The basis of dating for archeomagnetism has been provided in most cases either by radiocarbon ages or by archeological and historical data. Records of virtual axial dipole moments (VADMs) from North America over the last 2000 years [4,5] resemble a half-cycle sine curve with a minimum around A.D. 900 (Fig. 1). VADM values for potsherds from Ontario and Quebec from the tenth to the fifteenth centuries are, however, lower than values from the southwestern USA.

The aim of the present study was to measure the paleofield intensity recorded by potsherds from a Princess Point site in southern Ontario dated at A.D. 1030. This point provides a test of the low VADM values recorded elsewhere in Ontario about this time.

* Corresponding author. Tel.: 1-905-828-5336; Fax: 1-905-828-3717; E-mail: carvallo@physics.utoronto.ca

0012-821X/01/$ – see front matter
PII: S0012-821X(01)00259-X

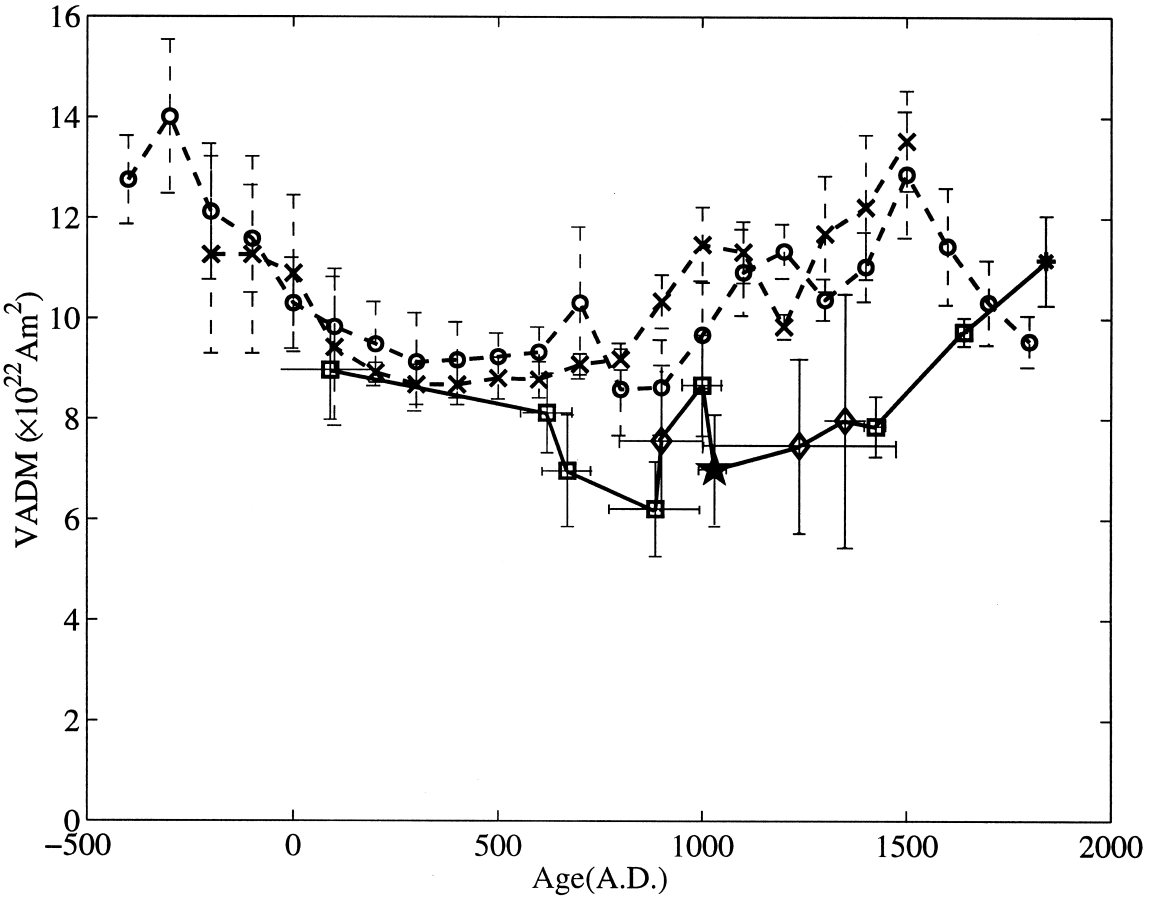

Fig. 1. VADM variations in northeastern and southwestern North America. Data are from: circles: Sternberg [5]; crosses: Lee [25], Parker [26], and Champion [27]; squares: Yu et al. [4]; asterisk: Dunlop and Zinn [2]; diamonds: Arbour and Schwarz [3] (after Yu et al. [4]); solid star: this study. The dotted lines show the trends for USA data, the solid line the trend for Quebec and Ontario data.

2. Samples

The samples used for this study come from Grand Banks, a Princess Point native site in southern Ontario (Fig. 2). Princess Point is identified as the ancestor of later Iroquoian societies in this region, and corresponds to a chronology from A.D. 500 to 1000 according to calibrated radiocarbon assays for different Princess Point sites in southcentral Ontario [6]. Pottery style is usually characterized by the presence of a cord-wrapped stick decoration on the exterior and/or the interior of the pot (D. Smith, personal communication).

The lithostratigraphy is characterized by two paleosols [7]. The upper paleosol (PII) is 15–20 cm thick and is buried under massive silt about 40 cm thick. An earlier paleosol (PI) occurs at some places at a depth of 1.2–1.7 m. Over 56 000 artifacts have been recovered from the site to date, mostly pottery fragments and chert flakes. The 24 pottery fragments used for this study were found in a pit about 1 m deep by 1 m in diameter. It is possible that multiple fragments belong to the same vessel.

The paleosols were dated by AMS radiocarbon assays on maize [6]. Five calibrated dates for PII have been obtained, indicating a chronology from

at least A.D. 500 to 1000. One of the dates was obtained on maize from the same pit as the pottery fragments used in this study. Assuming that the material in the pit corresponds to a single time of occupation, this dates the pottery to the range A.D. 990–1160 with a modal age of A.D. 1030. There could, however, be differences in ages of the different pottery fragments, since PII was continuously occupied for about 500 years. Moreover, pottery age corresponds to the moment when the pottery was broken and discarded, not the time of firing. Age uncertainty from this source is smaller, at most a few decades.

The pottery fragments were thin and fragile. They were therefore encased in plaster of Paris before drilling one or several 2.3 cm diameter cores from each sample. Each core was cut into 2.5 cm length specimens. A total of 76 specimens were prepared.

3. Anisotropy measurements

Anisotropy in ceramics has a significant influence on the acquisition of magnetization. In the present study anisotropy has two origins. Rogers et al. [8] explained the magnetic anisotropy in pottery as the result of fabric: preferential alignment of grains occurs during the moulding of the clay into shape, possibly further enhanced by grain growth during firing. However, the most important part of the anisotropy seems to originate from the irregular shape of our pottery fragments, which form an irregularly shaped magnetic source inside the non-magnetic plaster casing. Sample shape anisotropy is therefore significant. The fabric and sample shape anisotropies are combined in their effect and cannot be separated while being measured.

In order to avoid chemical changes caused by

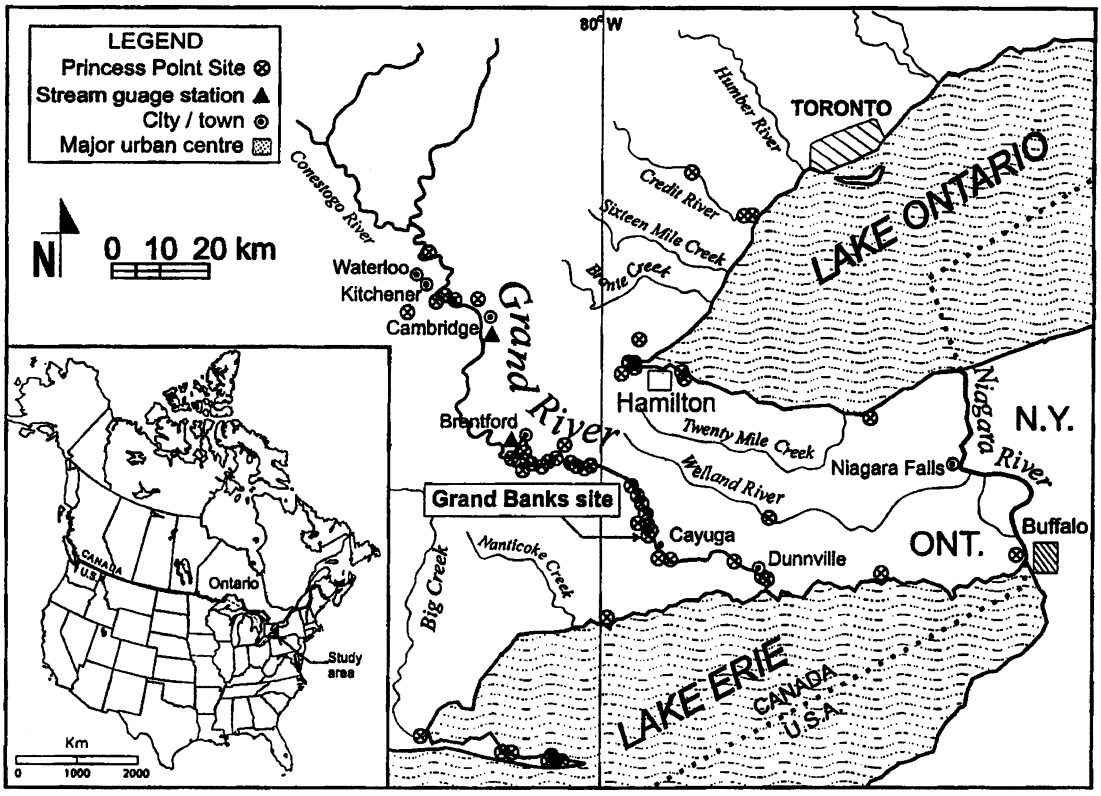

Fig. 2. Location of the archeological site sampled in this study (from Walker et al. [28]).

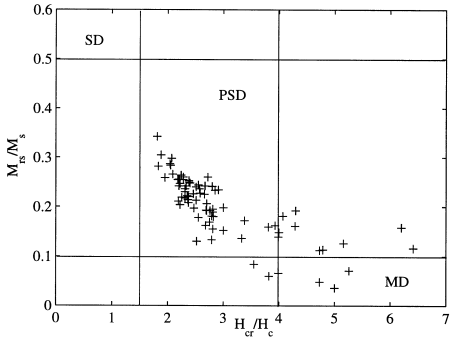

Fig. 3. Day plots for room-temperature hysteresis measurements.

the multiple heatings required to determine anisotropy of thermoremanent magnetization (TRM), the anisotropy of anhysteretic remanent magnetization (ARM) was measured instead [9]. ARM was produced with a Schonstedt alternating field (AF) demagnetizer. For each of the six directions ($\pm x$, $\pm y$, $\pm z$), the samples were first demagnetized in a peak field of 99.5 mT and their three components of magnetization were measured. Then they were given an ARM in an AF decreasing from 99.5 mT in the presence of a 30 μT steady field, and their magnetizations were measured again. For each of the six components, the vector difference of magnetizations between these two steps is a measurement of the ability to acquire an ARM in each direction. All measured magnetizations were corrected using the inverse AARM tensor [10].

4. Grain size characterization

4.1. Hysteresis parameters

Hysteresis in a maximum field of 0.5 T was measured on crushed separates using an alternating gradient force magnetometer. Hysteresis loops were obtained for 89 magnetic separates (three or four per potsherd). All the loops were corrected for paramagnetism.

Values of the hysteresis parameters M_{rs}/M_s and H_{cr}/H_c give insight into the distribution of domain states [11]. M_{rs}/M_s is 0.5 for samples containing only single-domain (SD) magnetite, and less than about 0.05 for multidomain (MD) bearing samples, while H_{cr}/H_c is more than about 4 for MD material. The majority of our samples fall in the pseudosingle-domain (PSD) range, with a few in the MD range (Fig. 3).

4.2. AF demagnetization

Eight specimens were AF demagnetized, in 11–17 field steps between 2.5 and 100 mT. Fig. 4 shows a typical result. The NRM is stable in direction after demagnetization to 15 mT, and the demagnetization curve has a sigmoid shape characteristic of SD or small PSD grains [12]. This conclusion is in agreement with the Day plot showing that these samples are in the PSD size range. The NRM intensity remaining after demagnetization to a peak field of 80 mT is between

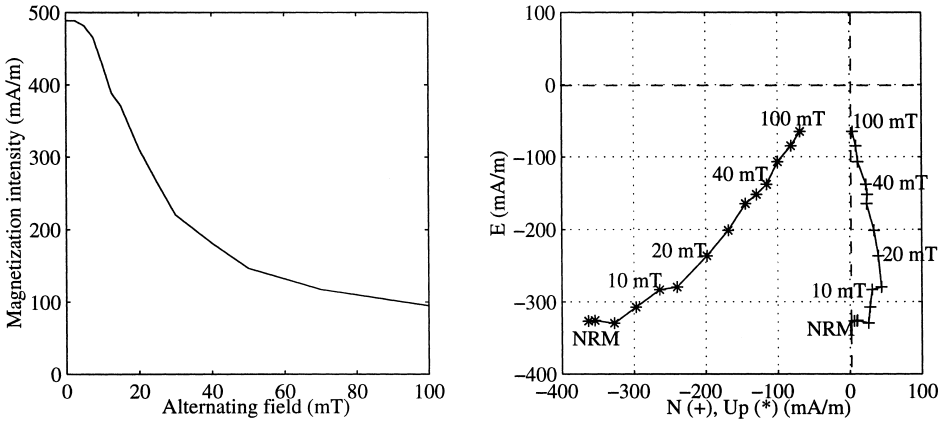

Fig. 4. Demagnetization spectrum and Zijderveld projections for AF demagnetization of sample H2.

10 and 25%. The median destructive fields (representing the coercivity of remanence) range from 20 to 30 mT.

5. Paleointensity determinations

5.1. Experimental procedure

The method applied in this study is the Thellier double-heating method [13] as modified by Coe[14]. The samples are first heated to a temperature T and cooled in zero field. The vector difference between the remanence after this step and the remanence after the previous zero-field step is the NRM lost. Then the specimens are heated again to the same temperature T and cooled in a laboratory field $H_{lab} = 29.8 \pm 0.2$ μT. The vector difference between the in-field and zero-field remanences at the same temperature step is the pTRM gained.

Sixty-three out of the initial 76 samples were selected for paleointensity determination. The samples were divided into three sets: two sets of 15 full-size samples heated under helium, with the intention of reducing oxidation during heating; and one set of 33 full-size and half-size samples heated in air.

Double heatings and coolings were performed in 11 steps from 250 to 580°C (in 50°C steps from 250 to 500°C, then 20°C steps from 500 to 560°C, and finally in 10°C steps from 560 to 580°C), using a MMTD furnace. Two pTRM checks were made for the in-air set, after the 560 and 580°C steps, repeating pTRMs at 540 and 560°C, and one for the in-helium sets, after the 580°C step, repeating pTRM at 560°C. Temperatures at specific locations inside the furnace were reproducible to within ±2°C.

Each heating–cooling step required 3–4 h. The samples were heated at a rate of 30°C/min, then held at the maximum temperature during 45 min, and finally cooled to room temperature at a rate of 30°C/min. Bulk magnetic susceptibility was measured using a Bartington AC bridge after each heating step in order to detect possible chemical alteration.

The same experimental procedure was also applied to four blank samples. NRM intensities were between 12 and 20 mA/m and less than 5 mA/m after demagnetization by heating to 350°C. pTRMs gained were less than 5 mA/m. These values are within the estimated 3–4% measurement error of typical specimen magnetizations.

5.2. Best fit determination and selection criteria

The best fit determination and statistical analysis of the results follow the least-squares fitting method described by York [15]. It uses the parameter S (quantity that is minimized by the fitting) defined by the sum of the squares of the weighted deviations of each data point from the best fit line:

$$S = \sum_i Z_i \, (y_i - b x_i - a)^2 \tag{1}$$

with:

$$Z_i = \frac{w(x_i) w(y_i)}{b^2 w(y_i) + w(x_i)} \tag{2}$$

where x_i and y_i are the measured values, $w(x_i)$ and $w(y_i)$ are the weights of the measured values, b is the slope, and a is the y-intercept of the best fit line.

The minimized factor S has a χ^2 distribution; its expectation value is $N-2$ (N being the number of points used in slope calculation) because two degrees of freedom, such as the slope and the y-intercept, have been used in line fitting. Then the quality factor S' defined by:

$$S' = \frac{S}{N-2} \tag{3}$$

has an expected value of 1 [4].

The quality factor S' is different from the quality factor q [16] or the dispersion coefficient s [17]. It has a statistical basis and rejection criteria can be set based on confidence limits.

The various parameters used as rejection criteria are as follows. The number N of points contained in the segment chosen to determine the paleointensity must be at least 6. The parameter f that measures what fraction of total remanence was destroyed in the segment used for the paleo-

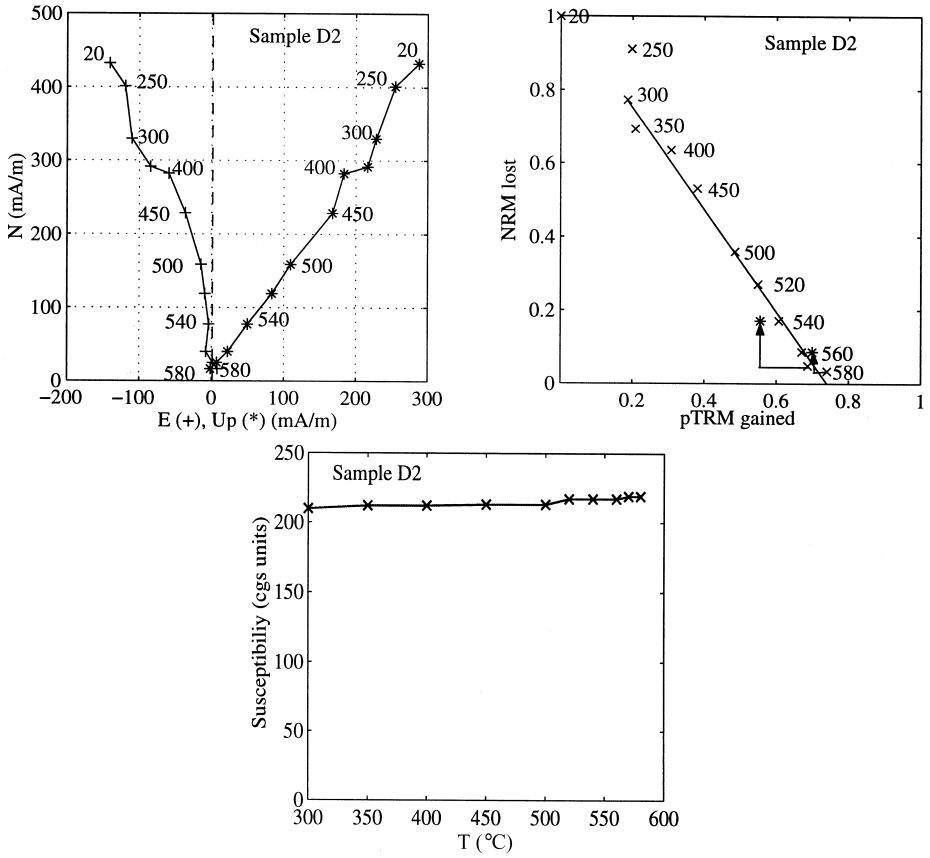

Fig. 5. Zijderveld diagram, Arai plot, and susceptibility variation for sample D2 (class I). The stars on the Arai plot represent the pTRM checks.

intensity determination must be more than 1/3. The quality factor S' defined above cannot exceed the quality factor defined for a 99% confidence limit based on a χ^2 distribution. Each pTRM check must be within $\pm 10\%$ of the original pTRM. Zijderveld projections [18] must show only one directional component in the temperature interval used for the paleointensity estimate. Finally, the variation of bulk susceptibility over the temperature interval used for the paleointensity estimate must be less than 10%. The gap factor g [16], measuring how evenly the data points were distributed, was calculated for each of these results but no selection criterion was based on this parameter.

The weight factor as defined by Yu et al. [4] was calculated as follows:

$$w = \frac{fg}{\sqrt{S'}\sigma_a\sigma_b} \quad (4)$$

where σ_b is the standard error in the slope and σ_a the standard error in the y-intercept calculated for the best fit.

5.3. Classification of samples

The decisive criterion for acceptance or rejection is the linearity of the Arai plot [19]. Samples that do not satisfy this criterion are definitively rejected. The directional criterion is evaluated using the paleomagnetism analysis programs provided by R.J. Enkin [20] and based on principal component analysis [21]. The precision index is provided by the maximum angular deviation

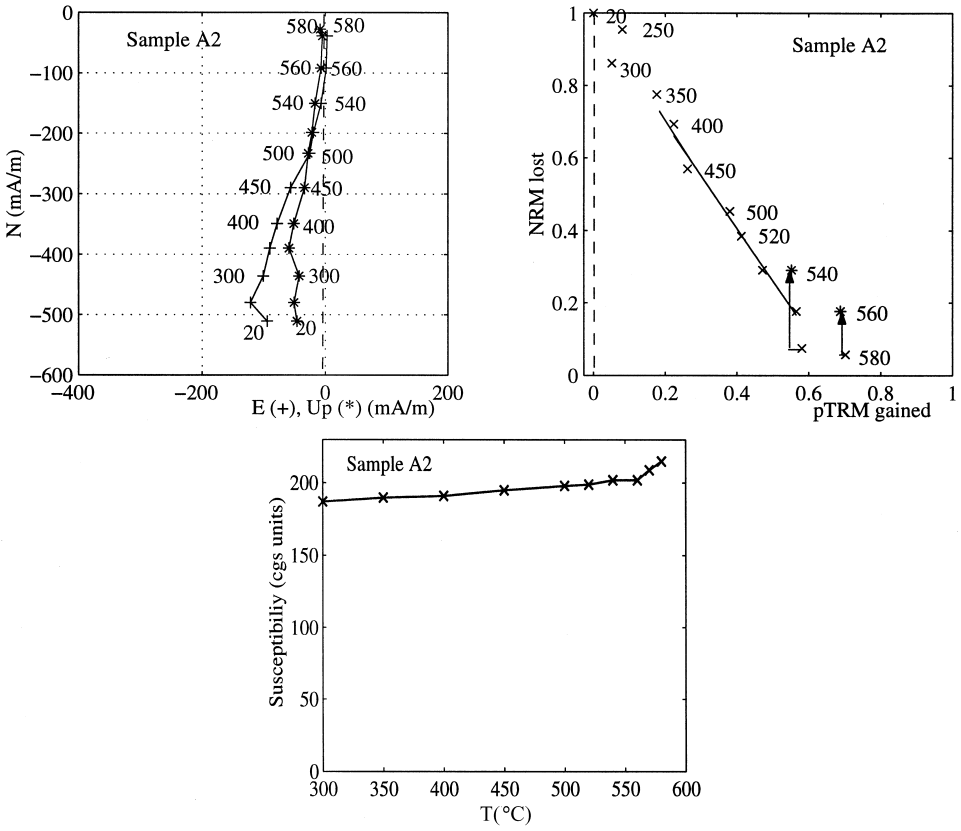

Fig. 6. Zijderveld diagram, Arai plot, and susceptibility variation for sample A2 (class II).

(MAD), which corresponds to the deviation of the direction if the fit along each axis is perturbed by one standard deviation. For this study, the rejection limit was fixed at MAD = 10°.

The accepted specimens are classified into two categories, depending on which selection criteria they satisfy. This classification gives insight into the quality and reliability of the results belonging to each class.

5.3.1. Class I

Class I specimens satisfy all the selection criteria. Twenty samples (16 from the set heated in air and four from the sets heated in helium) belong to this class. They represent the most reliable samples.

D2 is an example of such a specimen (Fig. 5). It shows ideal behavior in the NRM–pTRM plot. A viscous component is removed after heating to 300°C. Ten temperature steps (300–580°C), spanning 72% of the extrapolated NRM, are used for the paleointensity estimate. The quality of the line fitting is good, and pTRM checks have good repeatability. The bulk susceptibility varies only 4% over the interval 300–580°C.

5.3.2. Class II

Class II samples have no pTRM check in the temperature interval used for the paleointensity estimate, but show good linearity and satisfy the other selection criteria up to a temperature less than 560°C. Ten samples belong to class II, five from the set heated in helium and five from the set heated in air.

A typical class II example is sample A2 (Fig. 6): f, g, and S' have reasonable values in the interval 350–560°C, but there is no pTRM check to confirm that the sample did not experience any

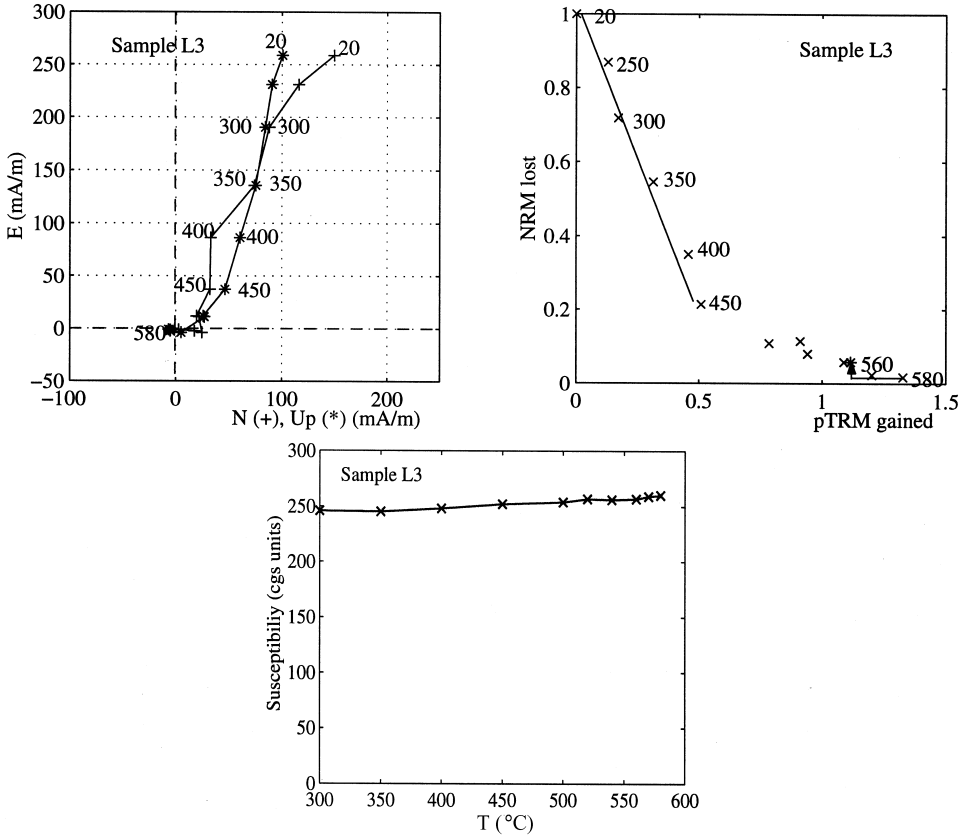

Fig. 7. Zijderveld diagram, Arai plot, and susceptibility variation for sample L3 (class II).

chemical transformation in this temperature interval. A unique direction is easy to identify, and the susceptibility varies only 5% over this temperature interval.

Among specimens from this category, a few have an NRM–pTRM plot showing two distinct linear segments, the second segment having a very shallow slope. L3 (Fig. 7) is an example of this kind of behavior. It is easy to identify two components, one in the range 20–450°C, having a steep slope, and the other one in the range 450–580°C, having a much smaller slope. However, the pTRM check done at 580°C shows good repeatability, and the bulk susceptibility does not vary significantly with temperature. These observations suggest that chemical changes are not the cause of the change in slope of the NRM–pTRM plot.

A possible explanation is that these potsherds were only heated to 450°C during firing. If so, the shallow slope would result from laboratory heating through a range where no NRM was originally acquired. The slope in this case is calculated using the segment below 450°C. Four specimens from potsherd L (L1, L2, L3, L4), and the three specimens from potsherd S (S1, S2, S3) have this type of behavior, although the majority of these samples were rejected for not satisfying the best fit parameter criteria.

5.4. Final results

The final results including all the relevant parameters are listed in Table 1. The weighted paleointensity average has been determined from class I and class II samples combined (30 samples). The dispersion about each mean is estimated using the standard deviation as defined by Coe et al. [16]:

Table 1
Paleointensity results for the accepted specimens

Specimen	N	ΔT (°C)	f	g	S'	w	$H \pm \sigma_H$ (μT)	MAD (°)	Class
A2	7	350–560	0.59	0.82	1.63	180	45.30 ± 2.11	3.6	II
A3	9	350–580	0.77	0.87	2.21	425	46.49 ± 1.67	5.0	I
A5*	9	250–560	0.71	0.81	1.57	326	52.15 ± 1.91	3.3	II
B2	7	400–570	0.50	0.82	1.86	134	42.91 ± 2.28	7.4	I
B4	9	350–580	0.73	0.88	2.21	418	37.25 ± 1.42	5.3	I
C2	8	400–580	0.67	0.86	1.50	314	43.21 ± 1.21	2.1	I
D1*	6	450–570	0.82	0.62	2.43	69	38.73 ± 2.47	5.1	II
D2	10	300–580	0.72	0.85	1.38	635	41.42 ± 1.25	4.1	I
E1	7	400–570	0.59	0.83	0.74	308	45.30 ± 1.99	4.7	I
E2	7	400–570	0.62	0.85	1.66	318	42.02 ± 1.69	8.3	I
E3*	8	350–570	0.72	0.83	2.44	212	47.98 ± 1.81	2.5	II
G3	9	350–580	0.84	0.91	2.20	734	34.27 ± 1.18	3.3	I
H1	7	450–580	0.51	0.63	0.90	127	36.36 ± 2.10	3.8	I
I2*	9	350–580	0.76	0.89	2.03	580	31.59 ± 1.18	5.0	I
J1	7	400–570	0.54	0.94	1.74	444	50.66 ± 2.72	5.4	I
J3	8	350–570	1.11	0.95	1.34	700	45.30 ± 1.87	3.3	I
L3*	6	20–450	0.77	0.79	2.36	35	45.59 ± 1.73	5.2	II
M1	6	450–570	0.55	0.85	0.48	490	29.50 ± 1.52	5.1	I
O1	8	300–560	0.73	0.85	1.25	462	45.89 ± 1.81	4.1	II
O2	8	300–560	0.70	0.85	0.76	529	47.68 ± 2.11	5.7	II
O3	8	300–560	0.80	0.85	0.88	929	30.69 ± 1.18	7.0	II
P1	9	300–570	0.68	0.87	1.02	444	49.17 ± 1.82	2.9	I
P2	6	500–580	0.37	0.76	0.32	97	37.55 ± 2.78	9.2	I
R2*	6	350–540	0.55	0.76	3.27	91	46.79 ± 2.46	4.6	II
T1	8	300–570	0.60	0.81	1.83	194	61.69 ± 2.31	5.1	I
T2*	6	500–580	0.50	0.89	2.45	208	32.78 ± 2.01	8.0	I
U1	8	300–560	0.74	0.86	2.41	512	40.23 ± 1.21	2.5	II
U2*	9	350–580	0.65	0.83	1.13	407	38.44 ± 1.48	5.7	I
X3*	9	300–570	0.65	0.84	2.42	412	33.64 ± 1.21	5.7	I
Y6*	7	450–580	0.57	0.77	0.82	210	40.23 ± 1.93	5.8	I
Average							42.04 ± 7.39		

Samples with an asterisk were heated in helium. Symbols are defined in the text.

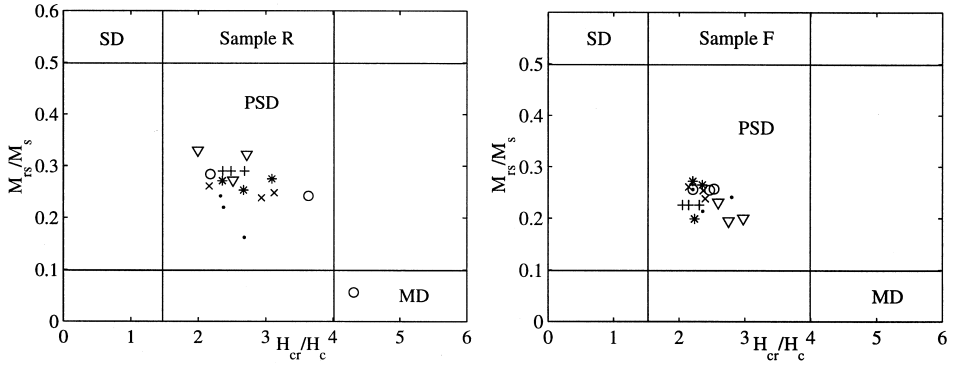

Fig. 8. Hysteresis parameters for the first experiment (see text). ·: room temperature measurements; ○: heating at 300°C; +: heating at 450°C; *: heating at 520°C; ×: heating at 560°C; ▽: heating at 580°C.

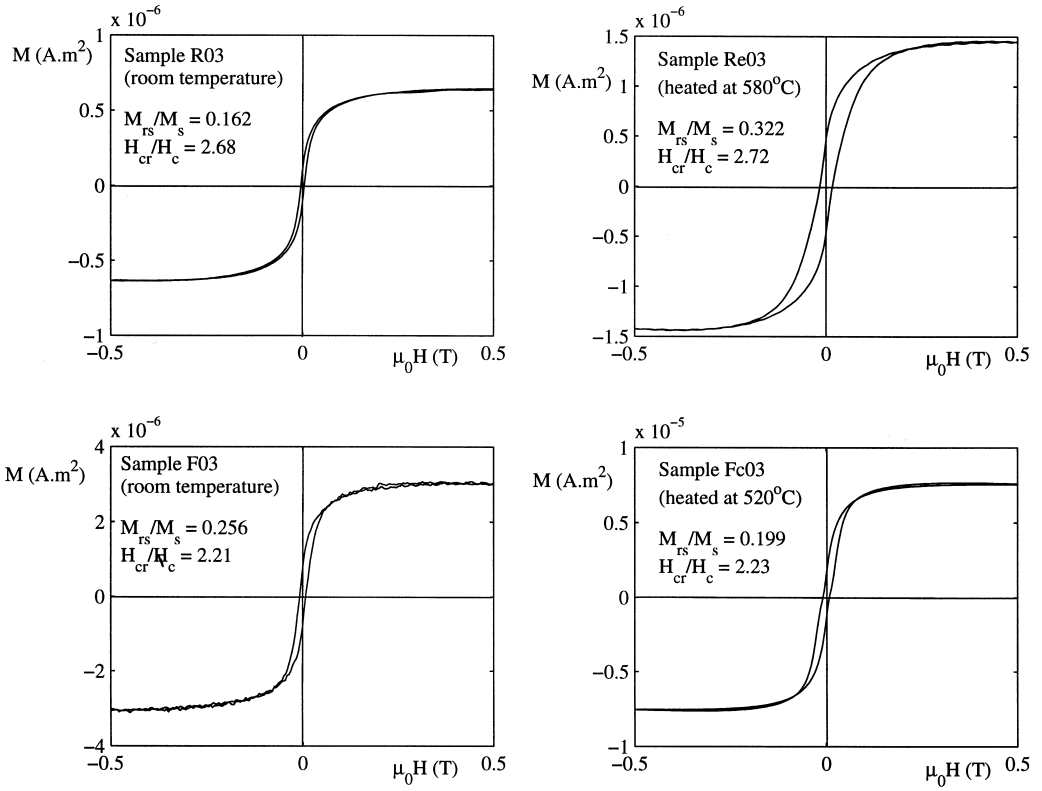

Fig. 9. Examples of hysteresis loops before and after heating. Top: sample R (heated in air); bottom: sample F (heated in helium).

$$\sigma_H = \sqrt{\frac{\sum_i (H_i - \overline{H})^2}{N-1}} \quad (5)$$

where H_i are the individual paleointensity values, $\overline{H}$ is the weighted mean paleointensity, and N is the number of samples.

In order to compare these values with paleointensities determined from areas at different latitudes, VADMs were calculated from the weighted mean paleointensities. The final results are: $H_a = 42.04 \pm 7.39$ μT; VADM = $7.01 \pm 1.31 \times 10^{22}$ Am^2.

5.5. Variation of hysteresis parameters as a function of heating temperature

In order to detect any change in the sample characteristics (mineralogy or size of the grains), hysteresis parameters were measured after various heating steps. Two different procedures were used.

5.5.1. Experiment 1

Five chips each of samples F and R were heated with the sample sets at 300°C. Then one chip of each sample was removed and the four remaining chips were heated with the sample sets to 450°C. One chip for each sample was again removed and the three remaining were heated to 520°C. One further chip was removed and the two others heated to 560°C. Finally, one chip was removed after this step and the last remaining chip for each sample was heated to 580°C. The R chips were heated in air, and the F chips in helium. Each chip experienced part of the same thermal treatment undergone by the samples used for paleointensity determination.

Each chip was then crushed and strong-field

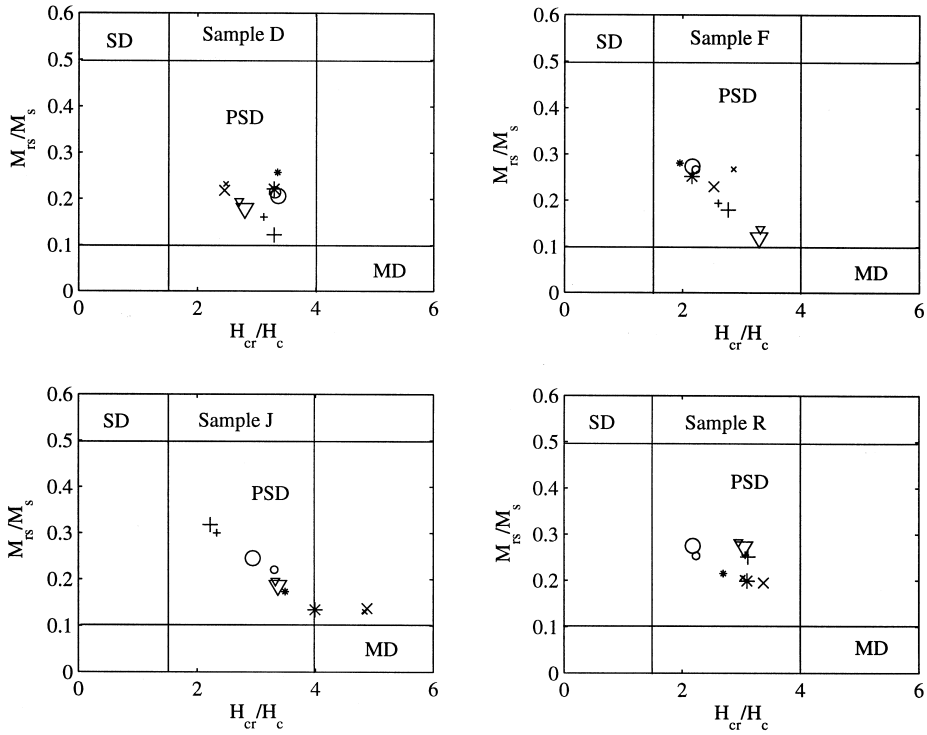

Fig. 10. Day plots for the second experiment (see text). ○: heating at 300°C; +: heating at 450°C; *: heating at 520°C; ×: heating at 560°C; ▽: heating at 580°C. The small symbols are the parameters measured before heating, the large symbols the parameters after heating.

hysteresis was measured on three magnetic separates per chip. Hysteresis parameters are plotted on a Day plot (Fig. 8). All the magnetic separates fall in the PSD range and there is no significant change in M_{rs}/M_s and H_{cr}/H_c with temperature, even within the PSD area.

However, the hysteresis loops become broader and more constricted for both F and R samples with increasing temperature (Fig. 9). Both features are manifestations of mixtures of magnetically soft and hard phases. A second, harder magnetic mineral is formed during heating (e.g. hematite), even though M_{rs}/M_s and H_{cr}/H_c remain constant.

5.5.2. Experiment 2

Four small pieces from different samples (J, R, D, and F) were crushed. Strong-field hysteresis at room temperature was then measured on five magnetic separates per piece. One separate per piece was then heated in air at 300°C, another one at 450°C, another one at 520°C, another at 560°C, and the last one at 580°C. Hysteresis parameters were remeasured after heating and compared with the previously measured values (Fig. 10).

Once again, almost all the samples have magnetic parameters that lie in the PSD range, and there is no significant change, for a given temperature, between the initial hysteresis parameters and the parameters measured after heating. The changes in M_{rs}/M_s and H_{cr}/H_c after heating are generally less than 10%.

However, the Arai plot for sample F3 has the concave shape that often accompanies chemical changes occurring during heating, and the bulk susceptibility shows a significant increase with heating. Measurements of hysteresis parameters after different heating steps do not reflect any of these changes.

6. Discussion

For some paleointensity studies, the difference between the cooling rate experienced by the magnetic material during its formation and the cooling rate used during the heating–cooling steps can introduce an important error in the paleointensity estimates [22]. Halgedahl et al. [23] showed by theoretical analysis that the cooling rate difference has to be larger than a factor of 700 to induce a difference larger than 20% in the paleointensity estimate. The rate used in the laboratory in the present study (30°C/min) is of the same order of magnitude as the rate that occurs during the firing of primitive pottery: pots fired by bonfire were allowed to cool 'naturally', which would correspond to about 4–6 h (D. Smith, personal communication). Therefore, no cooling rate correction was applied for this study.

Thirty samples out of 62 give reliable paleointensity results. The failure of the other samples could be due to a number of different causes. First, a poor reorientation of a specimen in the furnace in repeated heating steps, especially if the specimen was broken in the course of heating, could result in inconsistent behavior on the NRM–pTRM plot.

The concave curved shape of some Arai plots could be due to the presence of MD grains as remanence carriers. MD grains are quite rare in this study: Day plots show mainly PSD-like hysteresis parameters. However, sample N has MD-like parameters ($M_{rs}/M_s = 0.100$; $H_{cr}/H_c = 4.78$) consistent with the curved shape of the Arai plot. The other potential cause of this curved shape is mineralogical changes occurring at high temperatures. The hysteresis parameters do not show any significant variation as a result of heating; however, the increased coercivity and constricted shape of the hysteresis loops after heating testify to the formation of a new magnetically hard mineral.

Samples heated in helium have a higher rate of failure and bulk susceptibility variations than the samples heated in air. This is quite surprising, since it is generally believed that heating in an inert atmosphere should reduce the risk of oxidation and increase the chances of success. The cause of failure for our in-helium heatings is probably not the helium atmosphere per se but the use of closed sample holders which trap oxygen from the dewatering of the plaster of Paris.

However, Fig. 8 shows that the hysteresis parameters for the magnetic separates heated in helium appear to cluster more tightly than do the chips heated in air. This indicates that heating in helium may actually be useful.

The individual paleointensities have a fairly broad distribution. One reason for this could be that not all the pots were made at the same time. As the paleosol from which the potsherds were excavated was continuously occupied during 500 years, it is possible that the ages of these pottery fragments range over this interval or some part of it. However, the close spatial association of the fragments would argue against this. Moreover, two specimens drilled from the same pot do not show any better consistency. Samples P1 and P2, for instance, come from the same fragment, but the paleofield values for these samples are 49.17 ± 1.82 and 37.55 ± 2.78 μT.

The final paleointensity and VADM values for these samples dated at about A.D. 1030 are comparable to the values determined by Yu et al. [4] using Ontario potsherds dated between A.D. 600 and A.D. 1400, and are lower than results obtained from southwestern North America [5]. This trend confirms the presence of a substantial non-dipole field either in Ontario/Quebec or in southwestern North America. This non-dipole field would amount to as much as 40% of the total field at this time, whereas the present-day non-dipole field is only about 20% of the total field. Recent archeomagnetic intensity results from Denmark [24] show a low VADM value in the same period, suggesting that VADMs measured in southwestern North America are anomalously high.

7. Conclusions

The archeomagnetic study of potsherds from Grand Banks, Ontario, leads us to the following conclusions:

1. AF demagnetization and hysteresis measurements indicate that the remanence is carried by PSD grains.
2. Thirty reliable paleointensity measurements give a final VADM result of $7.0 \pm 1.3 \times 10^{22}$ Am^2 for these potsherds dated at about A.D. 1030.
3. This low value is in agreement with other low VADM values obtained from Ontario and Quebec sites compared to higher values from southwestern USA sites in this age interval.
4. Hysteresis parameters do not vary significantly as a result of heating.

Acknowledgements

We would like to thank Yong-Jae Yu, Özden Özdemir, Derek York, and Jerry Mitrovica for help and useful discussions, and David Smith for guidance and providing the archeological material. We thank Robert Sternberg and Peter Selkin for helpful reviews. This research has been supported by the Natural Sciences and Engineering Research Council of Canada through Grant A7709.*[RV]*

References

[1] E.J. Schwarz, K.W. Christie, Original remanent magnetization of Ontario potsherds, J. Geophys. Res. 72 (1967) 3263–3269.
[2] D.J. Dunlop, M.B. Zinn, Archeomagnetism of a 19th century pottery kiln near Jordan, Ontario, Can. J. Earth Sci. 17 (1980) 1275–1285.
[3] G. Arbour, E.J. Schwarz, Archeomagnetic intensity study of Indian potsherds from Quebec, Canada, J. Geomagn. Geoelectr. 34 (1982) 129–136.
[4] Y. Yu, D.J. Dunlop, L. Pavlish, M. Cooper, Archeomagnetism of Ontario potsherds from the last 2000 years, J. Geophys. Res. 105 (2000) 19419–19433.
[5] R.S. Sternberg, Archaeomagnetic paleointensity in the American Southwest during the past 2,000 years, Phys. Earth Planet. Interact. 56 (1989) 1–17.
[6] D.G. Smith, Radiocarbon dating the Middle to Late Woodland transition and earliest maize in Southern Ontario, Northeast Anthropol. 54 (1997) 37–73.
[7] G.W. Crawford, D.G. Smith, J.R. Desloges, A.M. Davis, Floodplains and agricultural origins: a case-study in South-central Ontario, Canada, J. Field Archeol. 25 (1998) 123–137.
[8] J. Rogers, J.M.W. Fox, M.J. Aitken, Magnetic anisotropy in ancient potteries, Nature 277 (1979) 644–646.
[9] M. Jackson, W. Gruber, J. Marvin, S. Banerjee, Partial anhysteretic remanence and its anisotropy: applications and grain size dependence, Geophys. Res. Lett. 15 (1988) 440–443.
[10] P.A. Selkin, J.S. Gee, L. Tauxe, W.P. Meurer, A.J. Newell, The effect of remanence anisotropy on paleointensity estimates: a case study from the Archean Stillwater Complex, Earth Planet. Sci. Lett. 183 (2000) 403–416.
[11] R. Day, M. Fuller, V.A. Schmidt, Hysteresis properties of titanomagnetites: grain-size and compositional dependence, Phys. Earth Planet. Interact. 13 (1977) 260–267.
[12] D.J. Dunlop, Ö. Özdemir, Rock Magnetism: Fundamentals and Frontiers, Cambridge University Press, New York, 1997, 573 pp.
[13] E. Thellier, O. Thellier, Sur l'intensité du champ magnétique terrestre dans le passé historique et géologique, Ann. Geophys. 15 (1959) 285–376.
[14] R.S. Coe, Paleointensities of the Earth's magnetic field determined from Tertiary and Quaternary rocks, J. Geophys. Res. 72 (1967) 3247–3262.
[15] D. York, Least squares fitting of a straight line with correlated errors, Earth Planet. Sci. Lett. 5 (1969) 320–324.
[16] R.S. Coe, C.S. Grommé, E.A. Mankinen, Geomagnetic paleointensities from radiocarbon-dated lava flows on Hawaii and the question of the Pacific non-dipole low, J. Geophys. Res. 83 (1978) 1740–1756.
[17] M. Prévot, E.A. Mankinen, R.S. Coe, C.S. Grommé, The Steens Mountain (Oregon) geomagnetic polarity transition, 2. Field intensity variations and discussion of reversal models, J. Geophys. Res. 90 (1985) 10417–10448.
[18] J.D.A. Zijderveld, A.C. demagnetization of rocks: analysis of results, in: D.W. Collinson, K.M. Creer, S.K. Runcorn (Eds.), Methods in Paleomagnetism, Elsevier, Amsterdam, 1967, pp. 254–286.
[19] T. Nagata, Y. Arai, K. Momose, Secular variation of the geomagnetic total force during the last 5000 years, J. Geophys. Res 68 (1963) 5277–5282.
[20] http://www.pgc.nrcan.gc.ca/tectonic/enkin.htm.
[21] J.L. Kirschvink, The least square line and plane and the analysis of paleomagnetic data, Geophys. J. R. Astron. Soc. 62 (1980) 699–718.
[22] J.M.W. Fox, M.J. Aitken, Cooling-rate dependence of thermoremanent magnetization, Nature 283 (1980) 462–463.
[23] S.L. Halgedahl, R. Day, M. Fuller, The effect of cooling-rate on the intensity of weak-field TRM in single domain magnetite, J. Geophys. Res. 85 (1980) 3690–3698.
[24] M. Gram-Jensen, N. Abrahamsen, A. Chauvin, Archaeomagnetic intensity in Denmark, Phys. Chem. Earth (A) 25 (2000) 525–531.
[25] S.S. Lee, Secular Variation of the Intensity of the Geomagnetic Field during the past 3,000 Years in North,

Central and South America, Ph.D. Dissertation, University of Oklahoma, Norman, OK, 1975, 220 pp.
[26] R.A. Parker, Archeomagnetic Secular Variation, M.Sc. Thesis, University of Utah, Salt Lake City, UT, 1976, 26 pp.
[27] D.E. Champion, Holocene geomagnetic secular variation in the western United States: implications for the global magnetic field, U.S. Geol. Surv. Open-file Rep., 1980, 80-824.
[28] I.J. Walker, J.R. Desloges, G.W. Crawford, D.G. Smith, Floodplain formation process and the archeological implications at the Grand Banks site, Lower Grand River, Southern Ontario, Geoarcheology 12 (1997) 865–887.